Method for Multi-Target Tracking Using a PHD-Filter in the Presence of Uncertain Probability of Detection

Rohith Reddy Sanaga and Carolin Frueh
School of Aeronautics and Astronautics, Purdue University,
rsanaga@purdue.edu, cfrueh@purdue.edu

ABSTRACT

Multi-target tracking using probabilistic finite set statistic methods, such as the Probability Hypothesis Density (PHD) filter, the Cardinality Probability Hypothesis Density filter (CPHD) or Multi-Bernoulli methods, are ubiquitously used for their advantageous properties of probabilistic data association in the presence of measurements that originate from real objects as well as clutter and their ability of probabilistic scene description in the absence of measurements. However, the performance of such methods crucially depends on their input parameters, such as the probability of birth and death of objects in the scene and the probability of detection and the clutter rate. While birth and death are of subordinate relevance in the SSA problem, and clutter usually can be well assessed on the sensor level, the probability of detection is a traditionally uncertain parameter. The probability of detection depends upon object properties, such as shape, attitude, and materials. While those are generally unknown for space debris objects, even active assets are subject to degradation over time in their optical properties. The probability of detection is hence a chronically uncertain parameter in the SSA multi-target tracking problem. Previous research has established that even slight deviations in the probability of detection lead to significantly degraded results. In this paper, a method is shown to include uncertainty in the probability of detection in the PHD filter framework. Using a Gaussian mixture representation of just five or seven components, significant improvements in the filter performance can be achieved. Several scenarios based on optical observations in the geosynchronous and geostationary transfer regime are shown.

1. INTRODUCTION

The space around Earth is becoming more crowded with increasing launches, a higher number of small satellites in orbit, and the proliferation of debris. Currently, there are around 44000 Earth-orbiting objects of a minimum size of 10 centimeters [15] that are catalogued. These objects consist of the active satellites and also space debris. Multi-target tracking (MTT) is the process of estimating the states, alongside the number of objects in any given region from clutter affected measurements (e.g. radar measurements, optical measurements). Historically, two major research approaches are used to explore the MTT regime, namely, the track-based approach and the population-based approach. The track-based approaches associate the measurements explicitly with the single targets to form a track.

The most well known representations of this approach is the Multi-Hypothesis filter and the Joint Probabilistic Data Association (JPDA) filter (introduced in [10]). Population-based approaches model all the objects in the scene as a single random entity and formulate the filtering problem using Finite Set Statistics (FISST) [20]. Both, track-based approaches and the population-based approaches have been researched in context of tracking in SSA ([12], [13], [24], [8], [14], [18], [19], ([4], [5]).

One of the important assumptions used in the formulation of GM-PHD filter is that the p_D is assumed to be known and constant, i.e., state-independent. Assumptions that appear to be valid in many tracking applications ([2], [1], [6], [26], [27]). However, this assumption cannot be justified in the observations of space objects. p_D is clearly orbital state-dependent because of the changing geometry of object, observer, and (either passive or active) illumination source. Secondly, the reflected illumination, either radar, laser, reflected sunlight, depends on the shape, attitude, and material of the object. While attitude might be relatively well known for active stabilized objects, material properties are known to change over time in the harsh space environment. For space debris objects, none of the parameters is well known. Hence, p_D has significant uncertainty associated with it and is not well known beforehand. Frueh [11]

shows that a model mismatch in p_D, the probability of detection, significantly degrades the performance of a simplified cardinality-only PHD filter.

In this paper, a new method is introduced modeling p_D, the probability of detection, via a Gaussian mixture approach, and incorporating it into the PHD tracking framework. Simulation results are shown for a ground-based optical tracking scenario. Using the Gaussian mixture approach for modeling p_D is shown to outperform classical PHD filter results using only 5 to 7 Gaussian components per object. A more comprehensive version of this paper has been submitted for journal publication and is currently under review.

2. GAUSSIAN MIXTURE PROBABILITY HYPOTHESIS DENSITY (GM-PHD) FILTER

The following equations constitute prediction and update equations of the PHD filter.

$$D_{k+1|k}(\mathbf{x}) = b_{k+1|k}(\mathbf{x}) + \int p_S(\mathbf{x}') f_{k+1|k}(\mathbf{x}|\mathbf{x}') D_{k|k}(\mathbf{x}') d\mathbf{x}' \tag{1}$$

$$D_{k+1|k+1}(\mathbf{x}) = \left(1 - p_D(\mathbf{x}) + \sum_{\mathbf{z}\in Z_{k+1}} \frac{p_D(\mathbf{x}) f_{k+1}(\mathbf{z}|\mathbf{x})}{\kappa_{k+1}(\mathbf{z}) + \int p_D(\mathbf{x}') f_{k+1}(z|\mathbf{x}') D_{k+1|k}(\mathbf{x}) d\mathbf{x}'}\right) D_{k+1|k}(\mathbf{x}) \tag{2}$$

The reader can refer to Chapter 16 of [20] for a detailed derivation of these equations. Here the subscripts $k, k+1$ refer to the time steps t_k, t_{k+1} respectively. $D_{k+1|k}$ is the predicted intensity and $D_{k+1|k+1}$ is the posterior intensity, $p_S(\mathbf{x}'), p_D(\mathbf{x})$ are probability of survival and probability of detection respectively, $b_{k+1|k}(\mathbf{x})$ is the PHD of the birth RFS which models the new objects entering a surveillance scene, $f_{k+1|k}(\mathbf{x}|\mathbf{x}')$ is the probability that a target with state $\mathbf{x}'$ at t_k transitions to a state $\mathbf{x}$ at t_{k+1} whereas $f_{k+1}(\mathbf{z}|\mathbf{x})$ is the probability that a target with state $\mathbf{x}$ generates a measurement $\mathbf{z}$ and $\kappa_{k+1}(\mathbf{z})$ is the intensity of the clutter RFS at time t_{k+1}.

Although the PHD filter dramatically reduces the computational complexity associated with the Multi-target Bayes filter, it does not provide an implementation. The GM-PHD filter [25], provides a closed-form solution to the PHD filter, assuming the probability of survival (p_S) and the probability of detection (p_D) are state-independent, among other assumptions.

2.1 birth PHD

In the space environment, it is difficult to predict when and with what state (position and velocity) the object will appear even probabilistically a priori. Information on object birth hence has to be shifted to the measurement step. Using admissible regions [21] in a Gaussian Mixture approximation [9] allows to incorporate birth for earth-orbiting objects, see Figure 1 for illustration. The admissible region Gaussian components are then translated into the state space. When

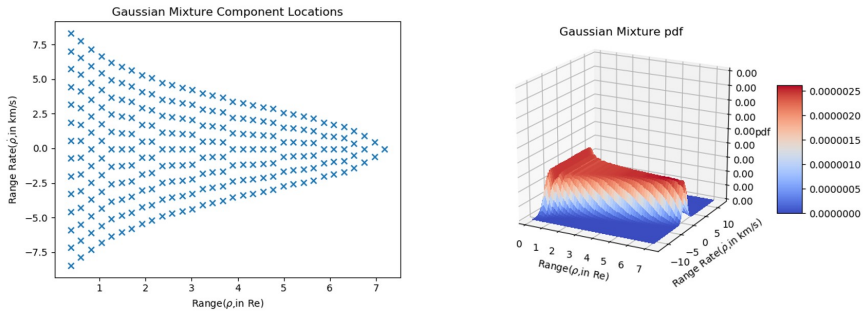

a) Location of GM components b) pdf of the Gaussian Mixture

Fig. 1: Gaussian Mixture approximation of an Admissible Region

the birth-PHD GM components are all obtained from the measurements, if these are added in the prediction step, as shown in equation (**??**) the update step would increase the weights of these components even if these components do not represent the targets, because all the components would, in theory, give the same predicted measurement which is equal to the true measurement. Therefore to avoid this ambiguity, the birth-PHD GM components are added in the

update step, which is the same as giving new initial components at this very time step. Technically, it is then equivalent to assume that there no new objects entering the scene, but the new targets (birth) are accounted for by adding new GM components (which have information on new objects) at each time step. The GM-PHD filter equations can then be written as:

$$D_{k+1|k}(\mathbf{x}) = D_{S,k+1|k}(\mathbf{x}) \tag{3}$$

$$D_{k+1|k+1}(\mathbf{x}) = (1-p_{D,k+1})D_{k|k-1}(\mathbf{x}) + \sum_{\mathbf{z}\in Z_{k+1}} D_{D,k+1}(\mathbf{x};\mathbf{z}) + b_{k+1|k}(\mathbf{x}) \tag{4}$$

3. PROBABILITY OF DETECTION (P_D) OPTICAL MEASUREMENTS

An analytical expression for p_D taking all of these factors into account. p_D can be expressed as ([22], [23]):

$$p_D = 1 - \frac{1}{2}\sum_{n=-\infty}^{\infty} \frac{\Gamma(n+1, \lambda_{obj}+\lambda_S+\lambda_D)}{n!}\left(erf\left(\frac{n+1-\mu_\varepsilon}{\sqrt{2g(\sigma_B^2+\sigma_R^2)}}\right) - erf\left(\frac{n-\mu_\varepsilon}{\sqrt{2g(\sigma_B^2+\sigma_R^2)}}\right)\right) \tag{5}$$

$$\mu_\varepsilon = tg + g/2 + \lambda_S + \lambda_D \tag{6}$$

$$t = 3 \times N(\text{ threshold, usually equal to 3-5 N}) \tag{7}$$

$$N = \sqrt{\frac{\lambda_{obj} + (1+\frac{1}{n})(\lambda_S + \frac{g^2-1}{12})}{g^2} + (1+\frac{1}{n})\sigma_R^2} \tag{8}$$

The quantity depending on the object is λ_{obj} which is the Poisson parameter of the object signal. λ_{obj} can be given as [3]:

$$\lambda_{obj} = (D-d)\frac{\bar{\lambda}}{hc} I_{obj}(\bar{\lambda}) \exp(-\tau(\bar{\lambda})R(\zeta))Q(\bar{\lambda})\Delta t g = k_{obj}A \tag{9}$$

$$I_{obj} = \int I_{Sun}(\lambda)\frac{A}{x_{topo}^2}\bar{\Psi}(\lambda)d\lambda \equiv \frac{I_0 A \Psi}{r_{topo}^2} \tag{10}$$

where D is the area of the aperture, d is the area of the obstruction of the aperture (secondary mirror), c is the speed of light, h is the Planck's constant, $I_{\lambda obj}(\lambda)$ is the object irradiation for a wavelength λ, τ is the atmospheric extinction coefficient and R is the atmospheric function (ζ is the elevation angle), Q is the quantum efficiency, g is the gain, I_0 is the solar constant, A is the reflecting area of the object, r_{topo} is the distance between the object and the observer and Ψ is the phase function of the object which encapsulates the reflecting properties of the objects. k_{obj} can be defined as the object number, entailing all parameters but area. The atmospheric model used in this work is $R = \frac{1}{\cos(\zeta)}$. If the object is spherical, Ψ is given as ([3]):

$$\Psi_{sphere} = \frac{2C_d}{3\pi}(\sin(\alpha) + (\pi-\alpha)\cos(\alpha)) \tag{11}$$

where C_d is the Lambertian Reflection coefficient and α is the angle between the relative position vector between Sun and the object and the relative position vector between the object and the observer.C_d is generally assumed to be a constant and value is taken at the mean wavelength.

3.1 State-Dependent p_D model

In order to implement a state-dependent p_D in the GM-PHD filter framework, [16] the new GM-PHD filter update equation becomes:

$$D_{k+1|k+1}(\mathbf{x}) = [1-p_D]D_{k+1|k}(\mathbf{x}) + \sum_{\mathbf{z}\in Z_{k+1}} D_{D,k+1}(\mathbf{x};\mathbf{z}) \tag{12}$$

where,

$$[1-p_D]D_{k+1|k}(\mathbf{x}) = \sum_{i=1}^{J_{k+1|k}} [1-p_{D,k+1}(m_{k+1|k}^{(i)})] w_{k+1|k}^{(i)} \mathcal{N}(x; m_{k+1|k}^{(i)}, P_{k+1|k}^{(i)}) \tag{13}$$

$$D_{D,k+1}(\mathbf{x};\mathbf{z}) = \frac{p_{D,k+1}(m_{k+1|k}^{(i)}) w_{k+1|k}^{(i)} q_{k+1}^{(i)}(z)}{\lambda c(\mathbf{z}) + p_{D,k+1}(m_{k+1|k}^{(i)}) \sum_{l=1}^{J_{k+1|k}} w_{k+1|k}^{(l)} q_{k+1}^{(l)}(\mathbf{z})} \tag{14}$$

For a resctricted Field of View (FOV) $p_{D,k+1}(m_{k+1|k}^{(i)})$ is taken to be zero if the estimated neab position (obtained from $m_{k+1|k}^{(i)}$) is not in the FOV.

3.2 Uncertainty in p_D

One major source of p_D are tumbling objects, exposing different reflective areas over time. Linearizing p_D relative to the area A, allows to determine the variance as:

$$\sigma_{p_D}^2 = \left(\frac{dp_D}{dA}\bigg|_{A=\mu_A} \sigma_A \right)^2 = \left(-0.5 \sum_{n=-\infty}^{\infty} \left(\frac{dP_1}{dA} P_2 + P_1 \frac{dP_2}{dA} \right) \sigma_A \right) \tag{15}$$

with:

$$\begin{aligned}
P_1 &= poisson.cdf(n,\lambda) \text{ where } \lambda = \lambda_{obj} + \lambda_S + \lambda_D \\
P_2 &= erf\left(\frac{n+1-\mu_\varepsilon}{\sqrt{2g(\sigma_B^2+\sigma_R^2)}} \right) - erf\left(\frac{n-\mu_\varepsilon}{\sqrt{2g(\sigma_B^2+\sigma_R^2)}} \right) \\
\frac{dP_1}{dA} &= \frac{-k_{obj} \exp(\lambda) \lambda^n}{n!} \\
\frac{dP_2}{dA} &= \frac{2}{\sqrt{\pi}} \exp(-z_1^2) \frac{dz_1}{dA} = \frac{2}{\sqrt{\pi}} \exp(-z_1^2) \frac{-g}{c} \frac{dt}{dA} \\
&\quad + \frac{2}{\sqrt{\pi}} \exp(-z_2^2) \frac{dz_2}{dA} = \frac{2}{\sqrt{\pi}} \exp(-z_2^2) \frac{-g}{c} \frac{dt}{dA}
\end{aligned}$$

with:

$$\frac{dt}{dA} = \frac{1.5 k_{obj}}{g^2} \left(\frac{\lambda_{obj} + (1+\frac{1}{n})(\lambda_S + \frac{g^2-1}{12})}{g^2} + (1+\frac{1}{n})\sigma_R^2 \right)^{-0.5}$$

$$c = \sqrt{2g(\sigma_B^2+\sigma_R^2)} \qquad z_1 = \frac{n+1-\mu_\varepsilon}{c} \qquad z_2 = \frac{n-\mu_\varepsilon}{c}$$

3.3 Validation of the model

As mentioned above, to verify the GM approximation and the linearized Jacobian of p_D, a Monte-Carlo analysis is done. Firstly, the probability distribution of the area is assumed to be Gaussian with $\mu, \sigma = 1, 0.3$. To test how good the Gaussian distribution fits the p_D distribution, 1000 samples of the area are drawn and p_D is calculated for each of the sample. A histogram is then plotted using 10 bins where the bin intervals are [0-0.1,0.1-0.2,...,0.9-1.0]. Then, the probability of p_D at the mid point of bin intervals [0.05,0.15,...,0.85,0.95] is calculated by taking the ratio of the number of samples in each bin to the total number of samples (1000). For Gaussian component splitting, splitting libraries have been used [7], [17]. Fig. 2 and 3 show the comparison of probability of p_D at the bin mid-points obtained via Monte-Carlo analysis and the Gaussian approximation. It can be seen from the plots that the Gaussian approximation is a very good even for small amounts of Gaussians.

For the implementation in the GM-PHD filter, $p_D(m_{k+1|k}^{(i)})$ in equations (13) and (14) is taken as the weighted average of the means of the Gaussian components i.e., the splitted Gaussian components of the area are first transformed to p_D space by the method described in section 3.2 and the p_D is assumed to then be equal to the weighted average of the means of the components. More precisely, if the probability distribution of p_D for a particular state $m_{k+1|k}^{(i)}$ is given by $\sum_{i=1}^{n} \alpha_i \mathcal{N}(p_D; \mu_i, \sigma_i^2)$ then $p_D(m_{k+1|k}^{(i)}) = \sum_{i=1}^{n} \alpha_i \mu_i$.

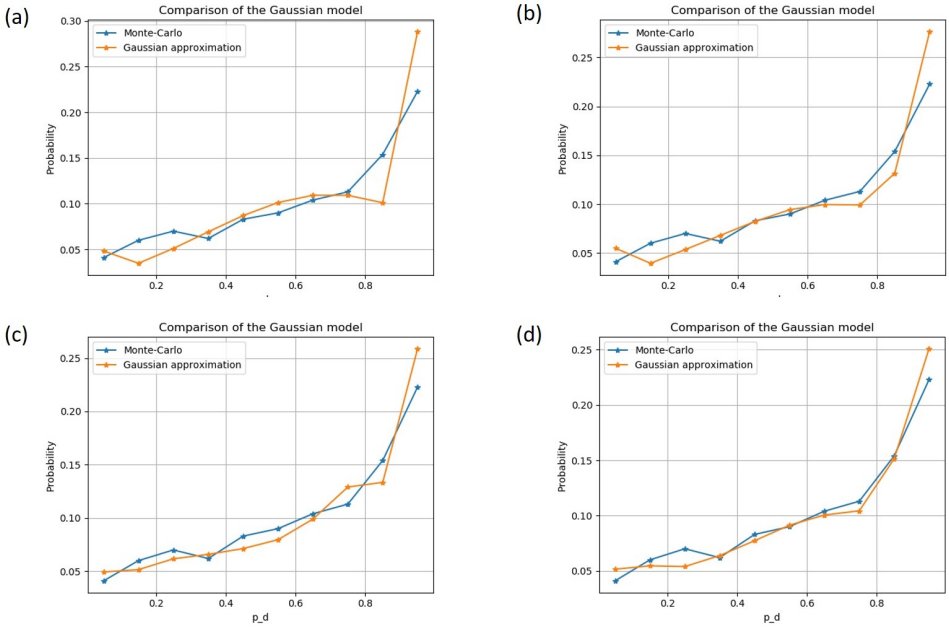

Fig. 2: (a) n = 1,(b) n = 3,(c) n = 4,(d) n = 5 at t=10

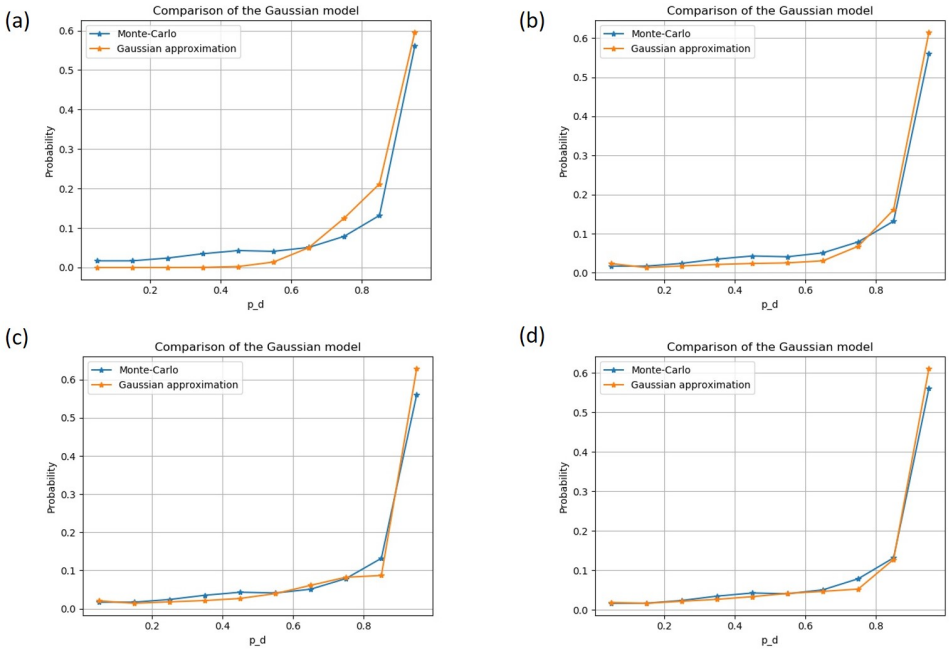

Fig. 3: (a) n = 1,(b) n = 3,(c) n = 4,(d) n = 5 at t=50

4. SIMULATION AND RESULTS

4.1 Validation of the Proposed Model

Two cases of simulations are used to validate the proposed GM-PHD filter variation for incorporating p_D uncertainty. The area (A) of the targets is assumed to be a random variable with a Gaussian distribution. The filter is run using three models of p_D for around 100 samples of area (100 sets of measurements), and the results are stored.

For the first model, namely "M1", the state-dependent p_D model is used where the area of the targets is assumed to be constant and equal to the mean of the Gaussian Distribution, disregarding any uncertainty in the probability of detection. For the second model "M2", the state-dependent p_D model is used but this time the value of p_D is taken as a extensive Monte Carlo weighted average i.e., samples of areas are drawn (from the Gaussian distribution), and p_D is calculated for each sample, and a histogram with 10 bins (0.0-0.1,0.1-0.2,...,0.9-1.0) is created, and, a weighted average using the centers of the bins is calculated. The method M2 is expected to be most exact, but it prohibitively computationally expensive.

The third model "M3" is the proposed model Gaussian Mixture model for representing the uncertainty in the probability of detection. As mentioned above, the filter is applied on the 100 sets of measurements, and the results for the state estimates and the cardinality (number of objects) estimates at each time step are stored. At each time step, an error is calculated using the Optimal Subpattern Assignment metric, also known as OSPA, The error is then averaged at each time step for all the samples, for all the models and the error is plotted.

4.1.1 Geostationary Objects Simulation

This scenario consists of two objects over 300 time steps with a step size of 1 minute. The observer is assumed to be on the surface of the Earth at a -91.44° longitude, and -7.15° latitude and measurements are taken at every time step and consist of topocentric angles and angle-rates. FOV is assumed to be $4^\circ \times 4^\circ$. It is assumed that the clutter Poisson parameter is 4. The probability of survival is constant and is assumed to be equal to 0.99. It is assumed that the target's area has a Gaussian Distribution with mean 1 and a standard deviation of 0.3. The objects time in FOV is given in Table 1 and Table 2 presents the initial states of the objects.

Table 1: Objects periods in FOV

Targets	Time steps in FOV
Object 1	0-177, 185-196
Object 2	80-147

Table 2: Orbital elements of targets

Targets	Semi-major axis (km)	Eccentricity	Inclination (rad)	Longitude ascending node (rad)	Argument of perigee (rad)	True Anomaly (rad)
Object 1	42164.455	0.00027	0.14278	0.80659	4.50221	0.18799
Object 2	42675.265	0.00178	0.22682	0.24389	4.53186	1.01972

Figure 4 shows the average OSPA error for the case described above with no clutter. Figure 4 shows that the model M2 and M3 performs better than model M1. M2 has the least error since it follows a Monte Carlo methodology. However, the performance of M2 is very similar to M2 and is also computationally less expensive. There is jump in the errors around the 80th time step because object 2 enters the FOV and an error corresponding to this object is added to the OSPA metric. The errors keeps on increasing after 200th time step because the objects are outside the FOV. Hence M1, M2, M3 give the same estimates of p_D.

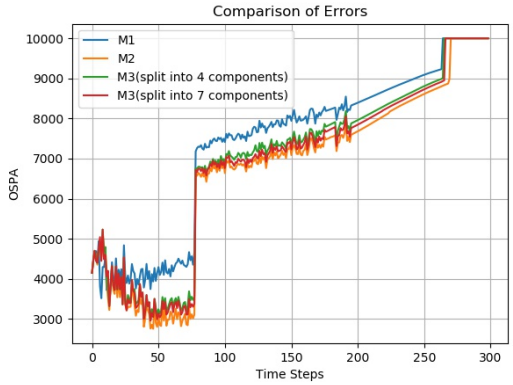

Fig. 4: Comparison of OSPA errors (Clutter not included)

The following figure (Fig.5) shows the results when clutter is included.

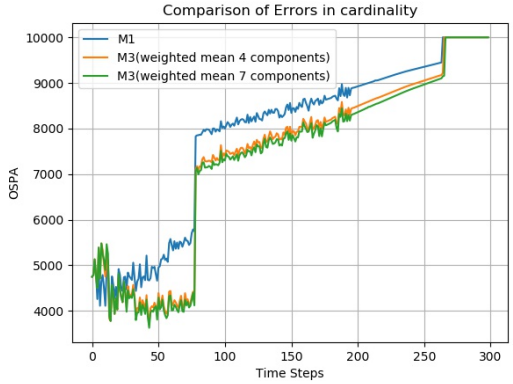

Fig. 5: Comparison of OSPA errors (Clutter included)

The same conclusions can be drawn again and it is seen that M3 performs better than M1 when there is an uncertainty in p_D.

4.1.2 LEO Objects Simulation

In this section, the targets are taken to be in LEO. This simulation is run for 135 time steps with a step size of 1 minute. The objects orbital elements are shown in Table 3. The observer is assumed to be on the surface of the Earth at a -91.44° longitude and -7.15° latitude and measurements are taken at every time step and consist of topocentric angles and angle-rates $(\alpha, \delta, \dot{\alpha}, \dot{\delta})$. The FOV is $16^\circ \times 16^\circ$. In the case of LEO objects, the observing telescope is assumed to follow a particular object and the FOV is then assumed to be a window around that object with a FOV of $;x^\circ \times y^\circ$. It is assumed that the clutter Poisson parameter is 4. Probability of survival is constant and is assumed to be equal to 0.99.

Table 3: Orbital elements of targets

Targets	Semi-major axis (km)	Eccentricity	Inclination (rad)	Longitude ascending node (rad)	Argument of perigee (rad)	True Anomaly (rad)
Object 1	7378.323	0.01034	1.44877	4.10412	4.01713	1.39263
Object 2	7849.591	0.05620	1.74179	3.53892	1.92272	1.97052
Object 3	7184.974	0.00870	1.45063	4.25730	2.65441	2.60532

Fig. 6 shows the results for this case.

Fig. 6: Comparison of errors (clutter not included)

It can be seen from Fig. 6 that the model M3 works better compared to the model M1. However, the error contrast at the end of the time interval (after the 40th time step) is not very high because the true p_D of the LEO objects used in the simulation is closer to one in the time interval considered.

5. CONCLUSION

A variation of the Gaussian Mixture Probability Hypothesis Density (GM-PHD) filter, which incorporates uncertainty in the probability of detection (p_D), is developed and validated using numerical simulations. GM-PHD filter, in its original form, models p_D as a state-independent quantity, i.e., a constant. It is seen that in the space environment, p_D is a state-dependent quantity and also has some uncertainty associated with it. This research successfully incorporated uncertainty in the p_D and also modeled p_D as a state (and therefore) time-dependent within the existing GM-PHD framework.

For the application in an SSA system, the birth was modeled via admissible regions, and an extended Kalman filter was used for orbit propagation and update. The objects were assumed to follow a two-body motion model, and for all the test cases, an optical ground-based single sensor scenario has been used. A variation of the GM-PHD filter, which models p_D as state-dependent, and which incorporates p_D uncertainty was developed. The uncertainty in p_D was created from uncertainty in the reflecting area of objects. The area of objects was assumed to be a Gaussian random variable. p_D is then linearly approximated by a Gaussian Mixture. The proposed method utilizes this to formulate an algorithm to incorporate p_D uncertainty in the GM-PHD filter. The proposed method to incorporate uncertainty was validated with simulations, and it was seen that it performs better than the filter, which does not accommodate uncertainty in p_D.

6. BIBLIOGRAPHY

REFERENCES

[1] Yaakov Bar-Shalom, Thomas E Fortmann, and Peter G Cable. Tracking and data association, 1990.

[2] Samuel S Blackman. Multiple-target tracking with radar applications. *Dedham, MA, Artech House, Inc., 1986, 463 p.*, 1986.

[3] J. McGraw C. Frueh, B. Little. Optical sensor model and its effects on the design of sensor networks and tracking. In *AMOS conference 2019, year=2019*.

[4] Y Cheng, KJ DeMars, C Früh, and MK Jah. Gaussian mixture phd filter for space object tracking. In *Proceedings of the AAS/AIAA Space Flight Mechanics Meeting, ser. Advances in the Astronautical Sciences*, 2013.

[5] Yang Cheng, Carolin Früh, and Kyle J DeMars. Comparisons of phd filter and cphd filter for space object tracking. 2014.

[6] Daniel Clark, Ba-Ngu Vo, and Judith Bell. Gm-phd filter multitarget tracking in sonar images. In *Signal Processing, Sensor Fusion, and Target Recognition XV*, volume 6235, page 62350R. International Society for Optics and Photonics, 2006.

[7] Kyle J DeMars, Robert H Bishop, and Moriba K Jah. Entropy-based approach for uncertainty propagation of nonlinear dynamical systems. *Journal of Guidance, Control, and Dynamics*, 36(4):1047–1057, 2013.

[8] Kyle J DeMars, Islam I Hussein, Carolin Frueh, Moriba K Jah, and R Scott Erwin. Multiple-object space surveillance tracking using finite-set statistics. *Journal of Guidance, Control, and Dynamics*, 38(9):1741–1756, 2015.

[9] Kyle J DeMars and Moriba K Jah. Probabilistic initial orbit determination using gaussian mixture models. *Journal of Guidance, Control, and Dynamics*, 36(5):1324–1335, 2013.

[10] Thomas Fortmann, Yaakov Bar-Shalom, and Molly Scheffe. Sonar tracking of multiple targets using joint probabilistic data association. *IEEE journal of Oceanic Engineering*, 8(3):173–184, 1983.

[11] C Frueh. Modeling impacts on space situational awareness phd filter tracking. *CMES-COMPUTER MODELING IN ENGINEERING & SCIENCES*, 111(2):171–201, 2016.

[12] C Frueh and T Schildknecht. Object image linking of objects in near earth orbits in the presence of cosmics. *Advances in Space Research*, 49(3):594–602, 2012.

[13] Carolin Früh. *Identification of Space Debris*. Shaker, 2011.

[14] Steven Gehly, Brandon Jones, and Penina Axelrad. An aegis-cphd filter to maintain custody of geo space objects with limited tracking data. In *Proceedings of the 2014 Advanced Maui Optical and Space Surveillance Technologies Conference*, pages 25–34, 2014.

[15] Loren Grush. *SpaceX just launched two of its space internet satellites — the first of nearly 12,000*, February 2018.

[16] Gustaf Hendeby and Rickard Karlsson. Gaussian mixture phd filtering with variable probability of detection. In *17th International Conference on Information Fusion (FUSION)*, pages 1–7. IEEE, 2014.

[17] Marco F Huber, Tim Bailey, Hugh Durrant-Whyte, and Uwe D Hanebeck. On entropy approximation for gaussian mixture random vectors. In *Multisensor Fusion and Integration for Intelligent Systems, 2008. MFI 2008. IEEE International Conference on*, pages 181–188. IEEE, 2008.

[18] Brandon A Jones, Steve Gehly, and Penina Axelrad. Measurement-based birth model for a space object cardinalized probability hypothesis density filter. In *AIAA/AAS Astrodynamics Specialist Conference*, page 4311, 2014.

[19] Brandon A Jones and Ba-Ngu Vo. A labeled multi-bernoulli filter for space object tracking. In *Proceedings of the 2014 AAS/AIAA Spaceflight Mechanics Meeting, Santa Fe, NM, USA*, pages 26–30, 2014.

[20] Ronald PS Mahler. *Statistical multisource-multitarget information fusion*. Artech House, Inc., 2007.

[21] Andrea Milani, Giovanni F Gronchi, Mattia de'Michieli Vitturi, and Zoran Knežević. Orbit determination with very short arcs. i admissible regions. *Celestial Mechanics and Dynamical Astronomy*, 90(1-2):57–85, 2004.

[22] Francois Sanson and Carolin Frueh. Noise quantification in optical observations of resident space objects for probability of detection and likelihood. In *AAS/AIAA Astrodynamic Specialist Conference, Vail, CO*, pages 15–634, 2015.

[23] Francois Sanson and Carolin Frueh. Noise estimation and probability of detection in non-resolved images: Application to space object observation. *Advances in Space Research*, 64(7):1432–1444, 2019.

[24] Navraj Singh, Joshua T Horwood, Jeffrey M Aristoff, Aubrey B Poore, Carolyn Sheaff, and Moriba K Jah. Multiple hypothesis tracking (mht) for space surveillance: Results and simulation studies. Technical report, AIR FORCE RESEARCH LAB KIRTLAND AFB NM SPACE VEHICLES DIRECTORATE, 2013.

[25] B-N Vo and W-K Ma. The gaussian mixture probability hypothesis density filter. *IEEE Transactions on signal processing*, 54(11):4091–4104, 2006.

[26] Ya-Dong Wang, Jian-Kang Wu, Weimin Huang, and Ashraf A Kassim. Gaussian mixture probability hypothesis density for visual people racking. In *2007 10th International Conference on Information Fusion*, pages 1–6. IEEE, 2007.

[27] Yun Zhang, Huilin Mu, Yicheng Jiang, Chang Ding, and Yong Wang. Moving target tracking based on improved gmphd filter in circular sar system. *IEEE Geoscience and Remote Sensing Letters*, 2018.